Numerical study on detonation initiation by multiple hot spots

Jie Sun[a], Pengfei Yang[b], Yiqing Wang[a], Zheng Chen[a,*]

[a]*HEDPS, CAPT, SKLTCS, College of Engineering, Peking University, Beijing 100871, China*
[b] *State Key Laboratory of High Temperature Gas Dynamics*, *Institute of Mechanics, Chinese Academy of Sciences, Beijing 100190, China*

Abstract

Detonation initiation is important not only for the development of advanced detonation engines and but also for the control of accidental explosion. There are mainly two types of detonation initiation, i.e., direct initiation and indirect initiation. This work focuses on direct detonation initiation which has a short initiation distance but requires large amount of energy deposition. Specially, we investigate the reduction in the critical initiation energy through replacing the single hot spot by multiple hot spots. The transient detonation initiation process in a stoichiometric $H_2/O_2/Ar$ mixture is examined through two-dimensional simulations considering detailed chemistry. It is found that under the same initiation energy, detonation initiation fails for a single large hot spot while successful detonation initiation can be achieved by employing six small hot spots. The collisions among adjacent transverse detonation waves induce new local explosions, which play a pivotal role in detonation initiation. To further assess the impact of wave collision, we change the hot spot energy used in the multiple hot spot configuration. For relatively low initiation energy, the blast wave quickly decays and decouples with the reaction zone. Consequently, the collision among transverse shock waves cannot induce new local explosion and detonation initiation fails. Increasing the initiation energy can enhance the blast wave and is favorable to the formation of local explosion, facilitating the rapid detonation initiation. Furthermore, the influence of hot spot number on detonation initiation is assessed. Interestingly the hot spot number is found to have non-monotonic effect on detonation initiation. Splitting a single hot spot into multiple hot spots enhances detonation initiation since the wave collision helps to induce local explosion. However, as the hot spot number increases, the energy of each hot spot is decreased and becomes excessively dispersed, which results in relatively weak blast wave and thereby weak wave interaction. Consequently, local explosion cannot be triggered and detonation initiation fails for relatively large hot spot numbers. This study provides insights on promoting detonation initiation through multiple hot spots.

Keywords: Detonation initiation; Critical initiation energy; Multiple hot spots; Shock wave collision

*Corresponding author. E-mail: cz@pku.edu.cn

Information for Colloquium Chairs and Cochairs, Editors, and Reviewers

1) Novelty and Significance Statement

The novelty of this work is that the transient detonation initiation process induced by multiple hot spots is investigated for the first time by simulations considering detailed chemistry. It is found that multiple hot spot helps to promote detonation initiation and thereby reduces the critical initiation energy. The underlying mechanisms are interpreted. Moreover, the effects of the initial initiation energy and hot spot number on detonation initiation processes are assessed and interpreted.

It is significant because this work demonstrates the feasibility of reducing the detonation initiation energy by using multiple hot spots. The collisions among adjacent transverse detonation waves are found to induce new local explosions and play a pivotal role in detonation initiation. It is shown that there is an optimum hot spot number for detonation initiation. Therefore, this study provides insights on promoting detonation initiation and reducing initiation energy through multiple hot spots.

2) Author Contributions

- Jie Sun: performed the research, analyzed the data, and drafted the manuscript.
- Pengfei Yang: aided in interpreting the results and revised the manuscript.
- Yiqing Wang: aided in interpreting the results and helped to design some figures.
- Zheng Chen: conceived the original idea, designed the research, and supervised the project.
- All authors discussed the results and contributed to the final manuscript.

3) Authors' Preference and Justification for Mode of Presentation at the Symposium

The authors prefer **OPP** presentation at the Symposium, for the following reasons:

- The novelty and significance of this work can be readily understood by the audience during oral presentation.
- The complicated wave interactions and local explosions can be more clearly illustrated by oral presentation.
- The transient detonation initiation process and the underlying mechanisms can be well presented by PPT.

1. Introduction

Detonation is a supersonic mode of combustion consisting of a shock wave coupled with a reaction zone [1]. Recently, detonation has received increasing attentions and has promising applications in advanced propulsion systems since it helps to achieve higher thermal efficiency and faster burning rate than deflagration [2]. Meanwhile, it is imperative to mitigate the occurrence of detonation in accident explosions since detonation has high overpressure and is extremely destructive [3]. Understanding detonation initiation is important not only for the development of advanced detonation engines and but also for the control of accident explosion.

Detonation initiation can be primarily categorized into indirect initiation and direct initiation [1]. Indirect initiation usually refers to the deflagration-to-detonation transition (DDT), which requires relatively low initiation energy but long initiation distance [4]. Direct initiation requires large amount of energy deposition so that detonation can be quickly formed [5]. One of the key parameters for direct detonation initiation is the critical initiation energy, E_C, which is an intrinsic property of a combustible mixture and depends on the mixture composition as well as the thermal conditions [1]. Successful direct detonation initiation is achieved only when sufficient energy is deposited, i.e., $E \geq E_C$.

In the literature, there are many studies on the measurement and prediction of critical initiation energy (see [6] and references therein). Here we focus on the endeavors to reduce the critical initiation energy and to promote detonation initiation. For example, it has been demonstrated that plasma discharge can be used to facilitate detonation initiation in pulsed detonation engines [7-9]. Plasma helps to produce active radicals and species (e.g., ozone) which can reduce the ignition delay time and thereby promote detonation initiation. Our previous work [10] examined how ozone addition affects detonation initiation, and showed that both ozonolysis reaction and ozone decomposition reaction help to reduce the critical initiation energy. The focusing effects of reflected shock waves can also help to initiate the detonation with lower initiation energy, which was demonstrated by simulations [11, 12] and experiments [13, 14].

Besides, spatial redistribution of the ignition is another effective way to reduce the critical energy for detonation initiation. Vasilev [15] reviewed the optimum ways for the detonation initiation process in terms of the spatial distribution of the input energy and proposed that multiple hot spots can promote detonation initiation. Guo et al. [16] simulated detonation initiation through dual-hot spot ignition and found that the collisions among adjacent shock waves induced by each hot spot can reduce the required initiation energy. Vasilev [17] measured the triple-point trajectory in a cylindrical detonation wave initiated by six hot spots. He found that detonation can initiated at lower initial pressure than the critical value by using the multiple hot spots. However, due to the limitation in experimental measurement, there is no detailed information on the characteristics of flow, reaction and wave interaction during the detonation initiation by multiple hot spots. Consequently, the underlying mechanisms of detonation initiation by multiple hot spots are not well understood. Besides, the influence of hot spot number and energy on detonation initiation have not been assessed. This motivates the present study.

This work aims to simulate and interpret the transient detonation initiation induced by multiple hot spots in a $H_2/O_2/Ar$ mixture. Specifically, we first compare the detonation initiation processes induced by a single hot spot and multiple hot spots, and assess the impact of multiple hot spots on the critical initiation energy. Then, the impact of the initial initiation energy on detonation initiation processes induced by multiple hot spots is examined. Finally, we assess the influence of hot spot number on detonation initiation. The remainder of the paper is organized as follows. The model and numerical methods are introduced in Section 2. After that the results are presented and discussed in Section 3. Conclusions are summarized in Section 4.

2. Model and numerical methods

We conduct two-dimensional simulations for the transient detonation initiation induced by different numbers of hot spot as depicted in Fig. 1. Since the present simulations are performed in 2D configuration, the initial hot spots can be identified as uniform line ignition sources perpendicular to the *x*-*y* plane.

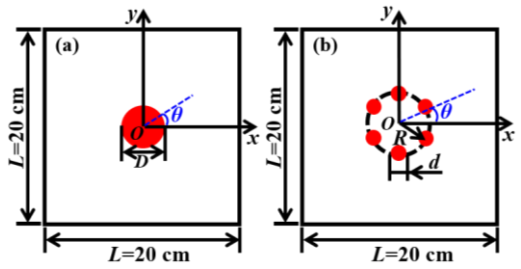

Fig. 1. Schematic of initial hot spot settings for (a) single hot spot and (b) multiple hot spots.

The computational domain is filled with static $H_2/O_2/Ar$ mixture (X_{H2}:X_{O2}:X_{Ar} = 2:1:7) of 300 K and 0.6 atm. Ar is used as the dilution gas to enhance the stability of the cellular detonation wave. The hot spot has the same $H_2/O_2/Ar$ mixture but has much higher temperature, T_h = 3000 K, and pressure denoted as P_h. We fix the total area of the hot spots, S_h,

$$S_h = \frac{\pi D^2}{4} = \frac{N\pi d^2}{4} = 6\pi \ (\mathrm{mm}^2) \qquad (1)$$

where D = 4.899 mm is the diameter of the single hot spot, and d and N are respectively the diameter and

number of hot spots in Fig. 1(b). Besides, the circumference radius of the hot spot center is fixed to be R = 3 mm for multiple hot spot configuration, which is closed to the hot spot radius for the single hot spot configuration (~2.45 mm). Note that this value may affect the detonation initiation process, which needs to be explored in future studies.

Due to symmetry, a quarter of the whole domain, i.e., $0 \le x \le 10$ cm and $0 \le y \le 10$ cm, is considered in simulations. Symmetric conditions are used at the boundaries of $x = 0$ and $y = 0$. The outflow conditions are used at boundaries of $x = 10$ cm and $y = 10$ cm. In simulations we consider the detailed hydrogen chemistry by Conaire et al. [18] which consists of 10 species and 21 elementary reactions. The transient detonation initiation process is simulated using the in-house code detonationFoam [19], which is developed based on OpenFOAM [20] and has been thoroughly validated for gaseous detonation simulation [19]. It has been successfully used in our previous studies on oblique detonation waves [21, 22]. The details on governing equations, numerical methods and code validation can be found in Ref. [19] and thereby are only briefly described below.

In detonationFoam, the finite volume method is used to solve the Euler equations for fully-compressible, multi-component reactive flows. The second-order MUSCL scheme with the pressure-corrected approximate Riemann solver, HLLC-P [23], is used to calculate the convective flux. The operator splitting approach is used so that the flow and chemical reaction processes are solved separately. The first-order Euler scheme is adopted for time advancement. The stiff ordinary differential equation solver, *seulex*, which employs an extrapolation algorithm based on the linearly implicit Euler method with step size control and order selection, is used to handle the chemical reaction [24]. Moreover, adaptive mesh refinement [25] and dynamic load balancing [26] are used to improve the computational efficiency.

To ensure grid convergence, we compare the results for detonation initiation by single hot spot predicted by simulations using three different grid sizes. For the cases shown in Fig. 2, the coarse grid sizes are 70.7 μm, 100 μm and 141.4 μm, respectively. All the cases use 3-level refinement mesh and the corresponding minimum grid size is 8.84 μm, 12.5 μm and 17.68 μm. For the simulation results, pressure distributions along the lines of θ = 0°, 0.1°, ..., and 90° are extracted, where θ is shown in Fig. 1. Then the average value of these pressure distributions is calculated to get the circumferentially-averaged pressure profile. Figure 2 shows that the circumferentially-averaged pressure profiles and triple-point trajectories predicted by different grid sizes are almost the same. Therefore, in all simulations we use the minimum grid size of 12.5 μm with the coarse grid size of 100 μm. The induction length for the $H_2/O_2/Ar$ mixture at 0.6 atm and 300 K is calculated to be 123.9 μm. Therefore, there are about 10 points within the induction zone for the grid size of $\delta x = \delta y$ =12.5 μm

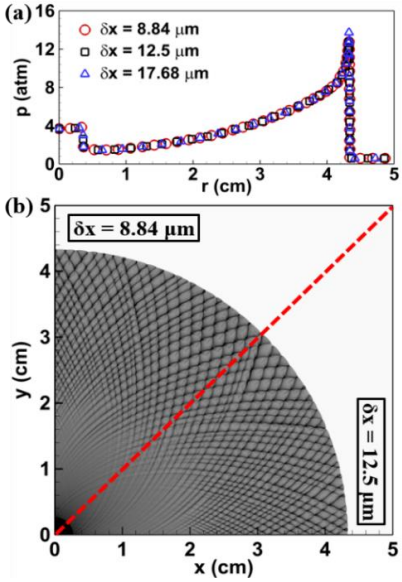

Fig. 2. (a) Distribution of the circumferentially-averaged pressure and (b) triple-point trajectories predicted by different grid sizes for single hot spot with P_h = 120 atm.

3. Results and discussion

3.1 Detonation initiation by a single hot spot

First, we simulate detonation initiation induced by a single hot spot with different initiation energies (which depends on the pressure of the hot spot, P_h). The temporal evolution of the pressure profiles, and normalized propagation speed of the leading shock wave along x-axis are shown in Fig. 3 for P_h = 120 atm and P_h = 35 atm.

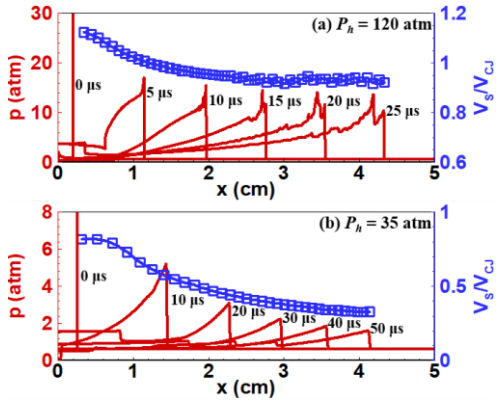

Fig. 3. The temporal evolution of the pressure profiles along x-axis and the change of normalized propagation speed of the shock wave with its position, Vs/V_{CJ}, for (a) P_h = 120 atm and (b) P_h = 35 atm. The Chapman-Jouguet (CJ) detonation speed for the $H_2/O_2/Ar$ mixture is V_{CJ} = 1686 m/s.

Successful detonation initiation is achieved for P_h = 120 atm and Fig. 3(a) shows that the shock speed gradually attenuates from the initial overdriven state to the steady-propagation state. Note that due to wave front curvature, the shock speed is slightly lower than Chapman-Jouguet (CJ) detonation speed. Besides, Figure 3(a) shows double-peak structures for the pressure profiles at t = 15, 20 and 25 μs. The first peak corresponds to pressure rise caused by the leading shock wave, while the second peak is caused by transverse wave. When the initial hot spot pressure is reduced to P_h = 35 atm, Fig. 3(b) shows that both the peak pressure and shock speed gradually decrease. At around t = 100 μs, the shock speed is only one-third of the CJ detonation speed (i.e., V_S/V_{CJ} = 0.33), indicating that the detonation initiation fails.

The above results show that failed detonation initiation occurs for a single hot spot with P_h = 35 atm. This will be used as a reference case for comparison with detonation initiation induced by multiple hot spots in the following subsection.

3.2 Detonation initiation by multiple hot spots

Here we use six hot spots (N = 6, d = 2 mm), as illustrated in Fig. 1(b), to initiate the detonation. According to Eq. (1), the amount of total initiation energy of the single hot spot (i.e., Fig. 1a, d = 4.9 mm) is equal to that of six hot spots (i.e., Fig. 1b) for the same P_h = 35 atm.

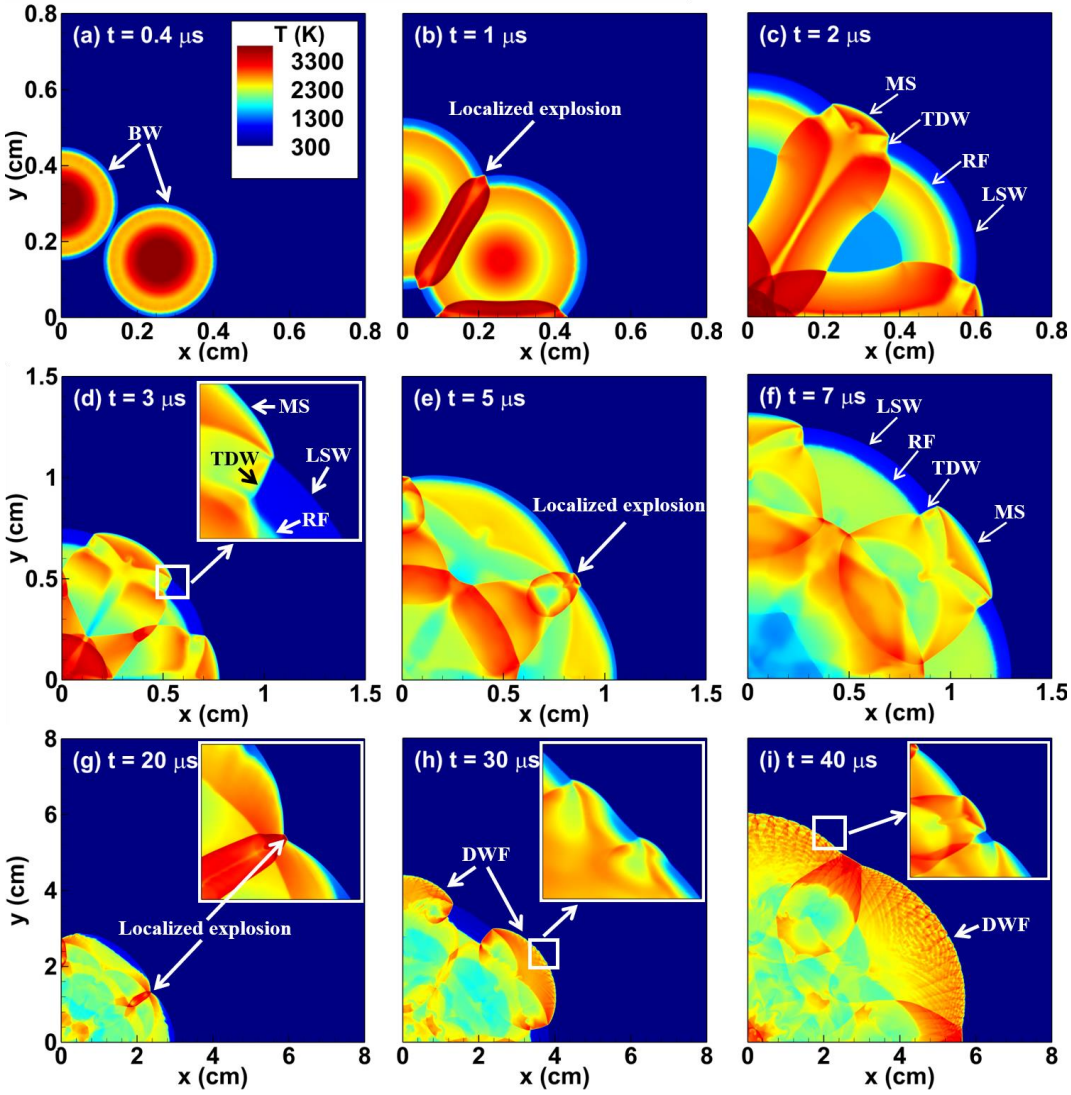

Fig. 4. The temporal evolution of temperature contour during detonation initiation induced by multiple hot spots with P_h = 35 atm. BW: blast wave; MS: Mach stem; TDW: transverse detonation wave; LSW: leading shock wave; RF: reaction front; DWF: detonation wave front. An animation of the whole detonation initiation process is shown in the Supplementary Material.

The detonation initiation process induced by six hot spots is shown Fig. 4. Due to symmetry only one and a half hot spots are shown. The whole initiation process can be divided into three stages. The first-stage evolutions are depicted in Figs. 4 (a-c). At t = 0.4 μs, Fig. 4(a) shows that the hot spots trigger rapid local autoignition, leading to the formation of diverging cylindrical blast waves (BW). The diverging BWs collide with each other, resulting in highly compressed regions with high pressure and temperature. This induces local explosion as shown in Fig. 4(b). The strong pressure waves induced by these local explosions further interact with arc shock waves originating from the initial hot spots, forming triple-wave structures consisting of Mach stem (MS), transverse detonation wave (TDW) and leading/incident shock wave (LSW), propagating outward as shown in Fig. 4(c). This first stage is mainly determined by hot spot autoignition and thereby it is referred to as the hot spot initiation stage.

The second stage evolutions are depicted in Figs. 4(d-f). Since the MS corresponds to relatively strong shock, chemical reactions immediately happen after the MS, and the distance between MS and the following reaction front (RF) is very small. On the contrary, the LSW has relatively low intensity and thereby there is a huge gap between the LSW and the RF (see Fig. 4d). As the triple-wave structures propagate, the transverse detonation waves spread towards both sides of the MS, consuming the mixture between the LSW and the RF (see Fig. 4d). Figures 4(c-e) shows that the width of the MS gradually increases and the MS evolves into a new LSW. The collision between two transverse detonation waves induces newly localized explosion as shown in Fig. 4(e), which then produces a new MS and a pair of TDWs propagating in the opposite directions as shown in Fig. 4(f). The next transition between MS and LSW, and the collision and reflection between a pair of TDWs continue during the propagating of the triple-wave structure. This is similar to the wave structure evolution occurring in cellular detonation. However, during this stage, the formation and evolution of the triple-wave structure is still determined by the initial hot spots. Therefore, this stage (3 μs < t < 20 μs) is referred to as the transition stage.

The third stage corresponds to the development and quasi-steady propagation of a circular expanding detonation as shown in Figs. 4(g-i). At t = 20 μs, Fig. 4(g) shows that the collision between a pair of TDWs induces local explosion. Figure 4(h) shows micro sub-structures appearing on the MS, indicating that the MS evolves into a typical circular diverging detonation wave front (DWF). At t = 40 μs, Fig. 4(i) shows that there are many micro triple-wave structures on the detonation wave front, indicating the formation of cellular detonation. Similar observations were reported and interpreted by Jiang et al. [27] and Shen et al. [28]. As the DWF propagates outwardly, its curvature decreases and thereby cellular instability develops, resulting in the generation of new transverse detonation waves [28].

Compared with the failed detonation initiation induced by a single hot spot shown in Fig. 3(b), successful detonation initiation is achieved by using multiple hot spots with the same total initiation energy as shown in Fig. 4. This shows that the multiple hot spots can effectively reduce the critical initiation energy. For the initiation process induced by a single hot spot, the cylindrical blast wave induced by the hot spot gradually attenuates due to the expansion effect, resulting in the decoupling between the leading shock wave and the reaction front, i.e., detonation initiation failure. However, for the initiation process by multiple hot spots, multiple blast waves are generated by the local autoignition triggered by each hot spot and the collisions between these blast waves induce local explosions, which play an important role in the achievement of successful detonation initiation.

Figure 5 shows the temporal evolution of wave front and the numerical soot foil during the successful detonation initiation by multiple hot spots. During the transition stage, it is seen that transverse detonation waves correspond to the high-pressure regions. In fact, the numerical soot foil records the transverse detonation wave trajectories, manifesting as fish-scale-like cell structure [29]. At t = 30 μs, cellular detonation wave has formed and small-scale detonation cells on DWF are clearly observed.

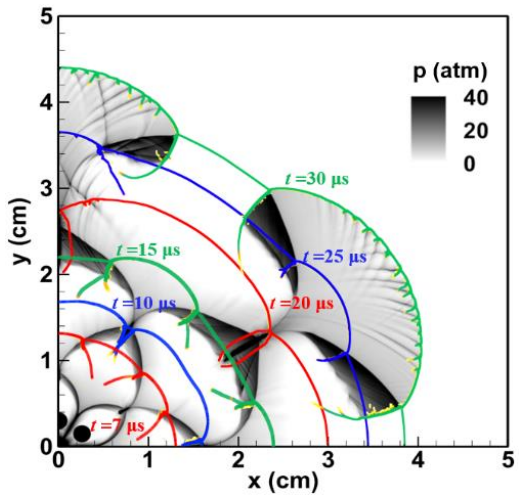

Fig. 5. Numerical soot foil for the case with 6 hot spots and P_h = 35 atm. The wave fronts at different times, t = 7, 10, 15, 20, 25 and 30 μs, are superimposed.

3.3 Effects of initiation energy

In the above two subsections, the hot spot pressure is fixed to be P_h = 35 atm. Here different hot spot pressures (i.e., different initiation energies) are considered and the detonation initiation processes are recorded in Fig. 6. Note that we still consider 6 hot spots with d = 2mm as depicted in Fig. 1(b).

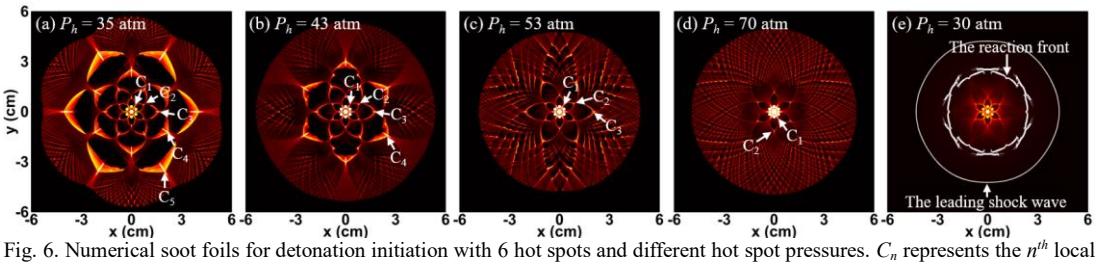

Fig. 6. Numerical soot foils for detonation initiation with 6 hot spots and different hot spot pressures. C_n represents the n^{th} local explosion caused by the collisions between adjacent blast waves. The animations of these detonation initiation processes are shown in the Supplementary Material.

Figure 6 shows the numerical soot foils for successful (Figs. 6a-d) and failed (Fig. 6e) detonation initiations. The results for $P_h = 35$ atm discussed in the previous subsection are plotted in Fig. 6(a). In Fig. 6, C_n represents the n^{th} local explosion caused by the collisions between adjacent blast waves. For an example, for $P_h = 35$ atm C_1 in Fig. 6(a) corresponds the collision and local explosion shown in Fig. 4(b).

With the increase of initiation energy or hot spot pressure, Figs. 6(a-d) shows that the cycle number of local explosion-blast wave decreases for the successful detonation initiation cases. Specifically, five, four, three and two cycle are respectively observed for $P_h = 35$, 43, 53 and 70 atm (Figs. 6 a-d). This is expected since the higher the hot spot pressure results in the stronger the blast waves and more intense collisions, which induce stronger local explosion and accelerate successful detonation initiation. Consequently, high initiation energy (or high hot spot pressure) facilitates the development of numerical disturbances between the leading shock wave and the reaction front, inducing transverse detonation waves and shortening the initiation distance, i.e., reducing the number of localized explosion-blast wave propagation cycles. As shown in the Supplementary Material, the numerical soot foil shown in Fig. 6(d) agrees qualitatively with the experimental results reported by Vasilev [15, 17]. In Fig. 6(e), detonation initiation fails for $P_h = 30$ atm. It is observed that the leading shock wave finally decouples with the reaction front.

In Fig. 7, we compare the evolution of circumferentially-averaged normalized shock wave speed V_S/V_{CJ} for different hot spot pressures. For successful detonation initiation, quasi-steady propagation is finally reached when V_S/V_{CJ} is slightly below, yet close to, unity. It is seen that before the quasi-steady propagation, there are several abrupt-acceleration-deceleration processes, which correspond to the local explosions, C_1~C_5, as shown in Fig. 6. For an example of $P_h = 35$ atm, the sudden increase of V_S at $t = 10.8$ μs is due to C_3 local explosion show in Fig. 6(a). Figure 7 also shows that the peak value of V_S caused by the same C_n local explosion increases with the hot spot pressure. This is mainly because higher initiation energy can induce stronger collisions and localized explosions. Note that the wave speed is calculated from the circumferentially-averaged value and that high wave speed can be achieved due to wave collision.

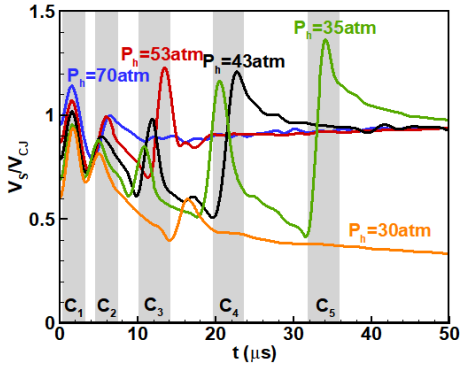

Fig. 7. The normalized propagation speed of the wave front, V_S/V_{CJ}, for different hot spot pressures. The local explosions, C_1~C_5 represent the local explosions depicted in Fig. 6.

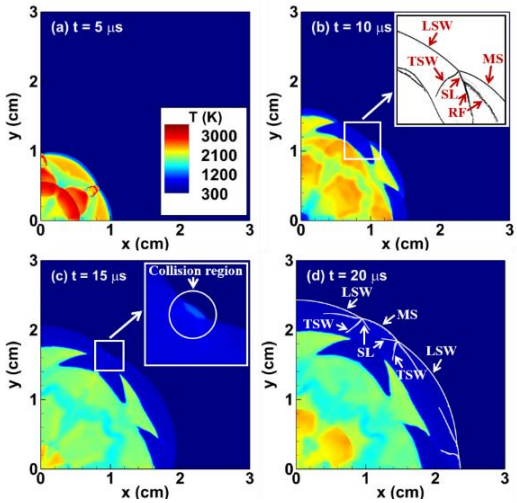

Fig. 8. Temperature contour for the failed detonation initiation with P_h = 30 atm. The wave structures are superimposed on (b) and (d). LSW: leading shock wave; MS: Mach stem; TSW: transverse shock wave; SL: slip line; RF: reaction front.

For case of $P_h = 30$ atm, Fig. 7 also shows that V_S decreases to $0.34V_{CJ}$ at $t = 50$ μs, indicating that

detonation initiation fails. For this case, the temperature contours and wave structures are shown in Fig. 8. At $t = 5$ μs, local explosion occurs. However, at $t = 10$ μs, the transverse shock wave (TSW) is shown to decouple with the RF. Subsequently, Fig. 8(c) shows that the collision between a pair of TSWs is not strong enough to induce new local explosion. Consequently, Fig. 8(d) shows that the distance between the leading shock waves and reaction zone further increases, resulting in the failure of detonation initiation.

3.4 Effects of initial hot spot number

In previous subsections, the hot spot number is fixed to be either $N = 6$ or $N = 1$. Here we assess the effect of hot spot number on detonation initiation with fixed total hot spot area of $S_h = 6\pi$ mm^2 and fixed hot spot pressure of $P_h = 35$ atm, i.e., the total initiation energy is unchanged.

Simulations for different hot spot numbers have been conducted. The results for hot spot number of $N = 2$, 4, 8, and 12 are present in Fig. 9. For $N = 2$ and 4, Figs. 9(a) and 9(b) show that fine cellular structures develop on the wave fronts. The propagation of triple-wave structures consisting of MS, TDW and LSW are clearly shown in the animation provided in the Supplementary Material. The wave fronts are found to tightly couple with the reaction fronts. Therefore, successful detonation initiation is achieved for $N = 2$ and 4. However, for $N = 8$ and 12 Figs. 9(c) and 9(d) show that the numerical soot foils decays significantly and are almost invisible in the region of $(x^2+y^2)^{1/2} > 3$ cm. Similar to results shown in Fig. 6(e) and Fig. 8(d), the reaction zone is found to decouple with the leading shock waves. Therefore, detonation initiation fails for $N = 8$ and 12.

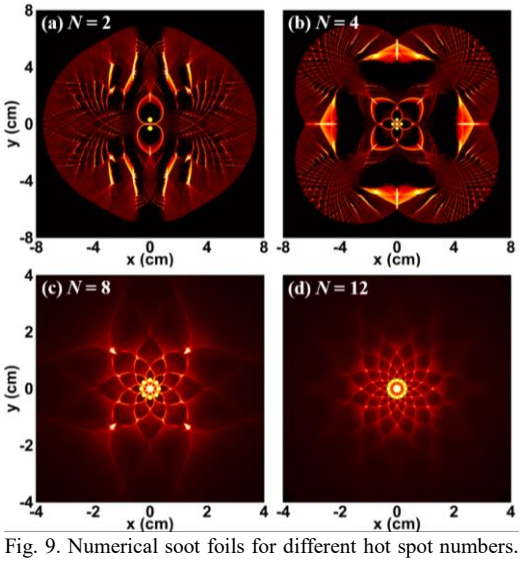

Fig. 9. Numerical soot foils for different hot spot numbers. P_h is fixed to 35 atm. The animations of these detonation initiation processes are shown in the Supplementary Material.

Figure 10 compares the circumferentially-averaged normalized propagation speed of the wave front, V_S/V_{CJ}, for $N = 1$, 2, 4, 6, 8 and 12. Similar to Fig. 7, Fig. 10 shows there are abrupt-acceleration-deceleration processes, in which the peak speed corresponds to the local explosion induced by wave collision ($C_1 \sim C_2$ for $N = 2$, $C_1 \sim C_4$ for $N = 4$ and $C_1 \sim C_5$ for $N = 6$). It is noticed that the time taken to reach the quasi-steady detonation propagation stage changes non-monotonically with the hot spot number: the shortest time is taken for $N = 2$ while the time for $N = 6$ is shorter than that for $N = 4$. Therefore, there is an optimum hot spot number for detonation initiation. For $N = 8$ and 12, Fig. 10 shows that V_S/V_{CJ} decreases continuously and thereby detonation initiation fails.

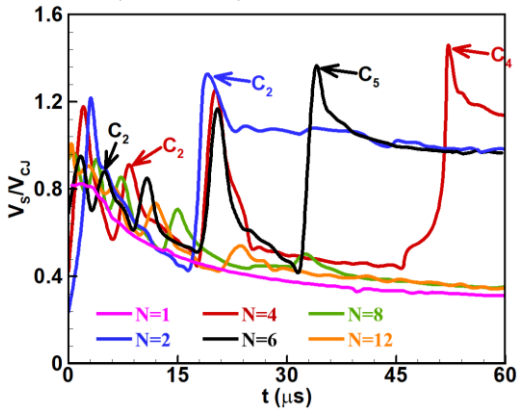

Fig. 10. The normalized propagation speed of the wave front, V_S/V_{CJ}, for different hot spot numbers. P_h is fixed to 35 atm.

The above results show that detonation initiation fails for $N = 1$, 8 and 12 but succeeds for $N = 2$, 4 and 6. Therefore, for the same initiation energy, the hot spot number N has a non-monotonic effect on detonation initiation. This can be explained as follows. As discussed in subsection 3.2, the local explosion induced by wave collision play an important role in detonation initiation by multiple hot spots. Increasing the hot spot number from $N = 1$ to $N = 2$ introduces wave collisions and localized explosions, which promotes the detonation initiation. However, for fixed total initiation energy, the strength each hot spot decreases with the increase of hot spot number. Consequently, wave collision and local explosion become weaker for larger hot spot number. This can be quantitatively elucidated by the decreasing local peak wave speed caused by C_2 collision, $V_S/V_{CJ} = 1.33$, 0.91 and 0.88 for $N = 2$, 4, and 6, respectively, as shown in Fig. 10. For relatively large hot spot number, $N = 8$ and 12, the strength of individual hot spot is not enough to induce strong local explosion, resulting in detonation initiation failure.

4. Conclusions

In this study, we conduct 2D simulations of detonation initiation by single hot spot and multiple hot spots in a stoichiometric $H_2/O_2/Ar$ mixture. First, we compare the detonation initiation induced by a single hot spot and by six hot spots with the same initiation energy. The detonation initiation process induced by multiple hot spots mainly consists of three stages: the hot spot initiation stage, the transition stage, and the detonation development and quasi-steady propagation stage. It is found that detonation initiation fails for the single hot spot but succeeds for six hot spots, demonstrating that multiple hot spot helps to promote detonation initiation and thereby reduces the critical initiation energy. This is due to the facts that the collisions among waves induced by multiple hot spots periodically introduce new local explosions, and these local explosions further enhance the wave intensity and accelerate chemical reaction and local autoignition. The coherent coupling between pressure waves and chemical reactions eventually induces self-sustained, circular detonation propagation with cellular structure on its front.

Then we assess the effects of initiation energy on detonation initiation by multiple hot spots. For fixed hot spot number of $N = 6$, increasing the initiation energy (hot spot pressure) can greatly reduce the number of cycles for local explosion occurring in the transition stage and thereby accelerate detonation initiation. This is because the higher the hot spot pressure, the stronger the blast waves and their collisions, which induce stronger local explosion and accelerate successful detonation initiation.

Finally, we examine the effect of hot spot number on detonation initiation under the same total initiation energy. Although splitting a single hot spot into 2, 4 and 6 smaller hot spots leads to a transition from the failed to successful detonation initiation, detonation initiation fails again when the hot spot number is increased to 8 and 12, indicating the effects of hot spot number on detonation initiation are non-monotonic. This is because for fixed total initiation energy, the strength of each hot spot decreases with the increase of hot spot number. Consequently, wave collision and local explosion becomes weaker for larger hot spot number and thereby detonation initiation fails for relatively large hot spot numbers.

This work helps to understand detonation initiation by multiple hot spots. In this work, we adopt uniform hot spots to initiate detonation and the initiation energy is determined by initial hot spot pressure. This setting is different from the practical applications. In future studies, it would be interesting to evaluate the detonation initiation process for multiple hot spot configurations considering more practical initiation methods. Besides, 2D simulations are conducted here while more complicated and stronger wave interactions are expected in 3D case, which need to be explored in future studies.

Supplementary materials

The animations of different detonation initiation processes are provided.

References

[1] J.H.S. Lee, The detonation phenomenon, Cambridge University Press, Cambridge, 2008.

[2] P. Wolański, Detonative propulsion, Proc. Combust. Inst. 34 (2013) 125-158.

[3] G. Ciccarelli, S. Dorofeev, Flame acceleration and transition to detonation in ducts, Prog. Energy Combust. Sci. 34 (2008) 499-550.

[4] E.S. Oran, V.N. Gamezo, Origins of the deflagration-to-detonation transition in gas-phase combustion, Combust. Flame 148 (2007) 4-47.

[5] L. He, P. Clavin, On the direct initiation of gaseous detonations by an energy source, J. Fluid Mech. 277 (2006) 227-248.

[6] B. Zhang, C. Bai, Methods to predict the critical energy of direct detonation initiation in gaseous hydrocarbon fuels – An overview, Fuel 117 (2014) 294-308.

[7] C. Cathey, F. Wang, T. Tang, A. Kuthi, M. Gundersen, J. Sinibaldi, C. Brophy, E. Barbour, R. Hanson, J. Hoke, F. Schauer, J. Corrigan, J. Yu, Transient plasma ignition for delay reduction in pulse detonation engines, AIAA-Paper 2007-443.

[8] J.K. Lefkowitz, Y. Ju, C.A. Stevens, T. Ombrello, F. Schauer, J. Hoke, The effects of repetitively pulsed nanosecond discharges on ignition time in a pulsed detonation engine, AIAA-Paper 2013-3719.

[9] D. Zheng, B. Wang, Acceleration of DDT by non-thermal plasma in a single-trial detonation tube, Chin. J. Aeronaut. 31 (2018) 1012-1019.

[10] J. Sun, B. Tian, Z. Chen, Effect of ozone addition and ozonolysis reaction on the detonation properties of $C_2H_4/O_2/Ar$ mixtures, Proc. Combust. Inst. 39 (2023) 2797-2806.

[11] N.N. Smirnov, O.G. Penyazkov, K.L. Sevrouk, V.F. Nikitin, L.I. Stamov, V.V. Tyurenkova, Detonation onset following shock wave focusing, Acta Astronaut. 135 (2017) 114-130.

[12] P.S. Utkin, A.I. Lopato, A.A. Vasil'ev, Mechanisms of detonation initiation in multi-focusing systems, Shock Waves 30 (2020) 741-753.

[13] Y. Li, B. Zhang, Visualization of ignition modes in methane-based mixture induced by shock wave focusing, Combust. Flame 247 (2023) 112491.

[14] Z. Yang, B. Zhang, Numerical and experimental analysis of detonation induced by shock wave focusing, Combust. Flame 251 (2023) 112691.

[15] A.A. Vasil'ev, Cellular structures of a multifront detonation wave and initiation, Combust. Explos. Shock Waves 51 (2015) 1-20.

[16] H. Guo, N. Zhao, H. Zheng, C. Sun, J. Yang, Numerical simulation of the direct initiation by double-point laser ignition, J. Combust. Sci. Technol. 01 (2021) 43-51.

[17] A.A. Vasil'ev, Dynamic Parameters of Detonation, in: F. Zhang (Ed.), Shock waves science and technology library, Vol. 6, Springer-Verlag Berlin, Heidelberg, 2012.

[18] M. Ó Conaire, H.J. Curran, J.M. Simmie, W.J. Pitz, C.K. Westbrook, A comprehensive modeling study of hydrogen oxidation, Int. J. Chem. Kinet. 36 (2004) 603-622.

[19] J. Sun, Y. Wang, B. Tian, Z. Chen, detonationFoam: An

open-source solver for simulation of gaseous detonation based on OpenFOAM, Comput. Phys. Commun. 292 (2023) 108859.
[20] OpenFOAM, https://openfoam.org.
[21] J. Sun, P. Yang, B. Tian, Z. Chen, Effects of wedge-angle change on the evolution of oblique detonation wave structure, Phys. Fluids 34 (2022) 096112.
[22] J. Sun, P. Yang, B. Tian, Z. Chen, Evolution and Control of Oblique Detonation Wave Structure in Unsteady Inflow, AIAA J. 61 (2023) 11.
[23] W. Xie, R. Zhang, J. Lai, H. Li, An accurate and robust HLLC-type Riemann solver for the compressible Euler system at various Mach numbers, Int. J. Numer. Methods Fluids 89 (2018) 430-463.
[24] E. Hairer, S.P. Nørsett, G. Wanner, Solving ordinary differential equations II: Stiff and differential-algebraic problems, second ed., Springer-Verlag, Berlin, 1996.
[25] D. Rettenmaier, D. Deising, Y. Ouedraogo, E. Gjonaj, H. De Gersem, D. Bothe, C. Tropea, H. Marschall, Load balanced 2D and 3D adaptive mesh refinement in OpenFOAM, SoftwareX 10 (2019) 100317.
[26] B. Tekgül, P. Peltonen, H. Kahila, O. Kaario, V. Vuorinen, DLBFoam: An open-source dynamic load balancing model for fast reacting flow simulations in OpenFOAM, Comput. Phys. Commun. 267 (2021) 108073
[27] Z. Jiang, G. Han, C. Wang, F. Zhang, Self-organized generation of transverse waves in diverging cylindrical detonations, Combust. Flame 156 (2009) 1653-1661.
[28] H. Shen, M. Parsani, The role of multidimensional instabilities in direct initiation of gaseous detonations in free space, J. Fluid Mech. 813 (2017) R4.
[29] X. Jia, Y. Xu, H. Zheng, H. Zhang, Direct detonation initiation in hydrogen/air mixture: effects of compositional gradient and hotspot condition, J. Fluid Mech. 970 (2023) A22.